

Physical Interactions of Simple Tools with JSC-1A Regolith Simulant

Brandon Tortorelli, Ted Rand, Steven Hackenburg

September 17, 2016

Abstract

As part of the NASA IMPACT program to model mechanical interactions with bodies in space such as comets, asteroids, and other Near Earth Objects (NEOs), the Colorado School of Mines team is designing a motor stage apparatus to interact with JSC-1A regolith simulant surfaces. This initial study involved development and testing of a prototype motor stage apparatus which was used to drive three types of probes into JSC-1A surfaces while collecting force data under standard Earth atmospheric conditions. The probes used were a conical-tipped probe, a wedge-tipped probe, and an anchoring probe. Main goals of the prototype system were to acquire general force trends for each interaction, and to isolate the most important design features for a more-complex in-vacuum system. Our data revealed force interactions that were very small in magnitude—on the order of tenths of Newtons—and more complex than our simple stiff beam probe and mount model could accurately predict. Our results lead us to recommend a more complex experimental model that can accurately represent deflection in the probes while also allowing for better measurement of regolith movement near the tip of the probes. Specifically, we recommend the following design features for the in-vacuum system: a load cell capable of measuring at very low ranges (thousandths of Newtons), reliability of structural axis alignment between trials, a robust mounting system that can accommodate each different type of probe, and consistency of sample preparation between trials.

List of Figures

1	Simple diagram of the experimental apparatus. The supporting electronic equipment such as motor controllers and supporting software are omitted.	9
2	Reference diagram for experimental model. The probe is modeled as a stiff beam centered along the vertical axis. The force on the probe from the JSC-1A is assumed to be a point force and moment applied directly at the tip of the probe and centered on the z-axis.	10
3	Photo of anchor entering regolith surface during preliminary test trial. Note - In later trials, a larger cup-shaped container replaced the metal hemisphere shown in an attempt to eliminate wall effects.	13
4	Schematic of anchor design with labeled dimensions. Units are in millimeters.	15
5	Compacted Trial 1: Vertical Force(N) Vs. Position (mm) of probe using a 6mm diameter probe on a compacted sample poured sample. The point of interaction line denotes where the probe first comes into contact with the simulant surface and the baseline is the 0 force axis. The position is based off of an absolute distance from the starting position of the probe. This trial hits a max force value of 0.46 ± 0.043 N	16
6	Poured Trial 1: Vertical Force(N) Vs. Position (mm) of probe using a 6mm diameter probe on a hand compacted sample. The point of interaction line denotes where the probe first comes into contact with the simulant surface and the baseline is the 0 force axis. The position is based off of an absolute distance from the starting position of the probe. This trial hits a max force value of 0.071 ± 0.043 N	17
7	Graph of horizontal force on the transducer for the .5 mm/s trials.	18
8	Graph of vertical force on the transducer for the .5 mm/s trials.	19
9	Graph of torque on the transducer for the .5 mm/s trials.	20
10	Plot of force in the z-direction over time increment of complete anchor trial with rotational speed $w=3.515$ rev/s. Magenta line marks when anchor probe stops movement and is completely submerged in regolith surface. Green line marks when anchor probe begins ascending from below the regolith surface.	21
11	Plot of force in the z-direction over time increment of complete anchor trial with rotational speed $w=3.45$ rev/s. Magenta line marks when anchor probe stops movement and is completely submerged in regolith surface. Green line marks when anchor probe begins ascending from below the regolith surface.	21
12	Plot of Force in Z-Direction with with no regolith trial to compare amounts of motor noise	22
13	Plot of three separate trials showing force in the Z-Direction during descent of the anchor into regolith sample at $w=3.515$ rev/s. Magenta line marks point when bottom tip of anchor probe first enters the regolith surface.	24
14	Plot of three separate trials showing force in the Z-Direction during ascent of the anchor out of the regolith sample. Magenta line marks point when bottom tip of anchor probe leaves the regolith surface.	24

15	Plot of three separate trials showing force in the Y-Direction during descent of the anchor into the regolith sample with speed $w=3.515$ rev/s. Magenta line marks point when bottom tip of anchor probe first enters the regolith surface.	25
16	Plot of three separate trials showing force in the Y-Direction during ascent of anchor out of regolith sample. Magenta line marks point when bottom tip of anchor probe leaves the regolith surface.	26
17	Plot of three separate trials showing torque about Y-axis during descent of anchor into regolith sample at speed $w=3.515$ rev/s. Magenta line marks point when bottom tip of anchor probe first enters the regolith surface.	27
18	Plot of three separate trials showing torque about Y-axis during ascent of anchor out of regolith sample. Magenta line marks point when bottom tip of anchor probe leaves the regolith surface.	27
19	Plot of three separate trials showing force in the X-Direction during descent of the anchor into regolith sample at $w=3.515$ rev/s. Magenta line marks point when bottom tip of anchor probe first enters the regolith surface.	32
20	Plot of three separate trials showing force in the X-Direction during ascent of the anchor out of the regolith sample. Magenta line marks point when bottom tip of anchor probe leaves the regolith surface.	32
21	Plot of three separate trials showing torque about X-axis during descent of anchor into regolith sample at speed $w=3.515$ rev/s. Magenta line marks point when bottom tip of anchor probe first enters the regolith surface.	33
22	Plot of three separate trials showing torque about X-axis during ascent of anchor out of regolith sample. Magenta line marks point when bottom tip of anchor probe leaves the regolith surface.	33
23	Plot of three separate trials showing torque about Z-axis during descent of anchor into regolith sample at speed $w=3.515$ rev/s. Magenta line marks point when bottom tip of anchor probe first enters the regolith surface.	34
24	Plot of three separate trials showing torque about Z-axis during ascent of anchor out of regolith sample. Magenta line marks point when bottom tip of anchor probe leaves the regolith surface.	34
25	Compacted Trial 2: Vertical Force(N) Vs. Position (mm) of probe using a 6mm diameter probe on a compacted sample poured sample. The point of interaction line denotes where the probe first comes into contact with the simulant surface and the baseline is the 0 force axis. The position is based off of an absolute distance from the starting position of the probe. This trial hits a max force value of 0.232 ± 0.043 N	35
26	Poured Trial 2: Vertical Force(N) Vs. Position (mm) of probe using a 6mm diameter probe on a hand compacted sample. The point of interaction line denotes where the probe first comes into contact with the simulant surface and the baseline is the 0 force axis. The position is based off of an absolute distance from the starting position of the probe. This trial hits a max force value of 0.055 ± 0.043 N	35

List of Tables

1	Table of peak force values across all conical probe trials.	18
---	---------------------------------------------------------------------	----

2	Accuracy error values and uncertainty ranges of the ATI Gamma transducer used in all experiments.	28
3	Preliminary cost analysis table for the "Physical Interaction of Simple Tools with the Surface of Airless Bodies" project	30

1 Introduction

Simple mechanical interactions with bodies in space, such as comets, asteroids, and other Near Earth Objects (NEOs), are not well understood because the basic properties of the regolith that composes these bodies have not been studied in great depth. Current models propose that cohesive and coulombic forces are the dominant forces holding NEOs together in microgravity environments [3]. However, the extent of these forces is not well characterized, hindering the development of optimized tools to interact with the surface of NEO bodies - possible sites for future space studies and resource mining. As part of the NASA IMPACT program, the Colorado School of Mines team will experiment with geometrically simple probes and interactions that can be extrapolated and applied to more complex systems. The experimental results can be used to support any future endeavors to study or attempt physical interactions with NEOS. Since a thorough understanding of mechanical interactions with regolith surfaces in space environments is essential for space science and commercial space endeavors, this project is necessary for the future of human space exploration.

Our initial study involves developing and testing a prototype motor stage apparatus which will be used to drive three types of probes into the surface of regolith simulant JSC-1A while collecting force data under standard Earth atmospheric conditions. These probes are a conical-tipped probe, a wedge-tipped probe, and an anchoring probe. Each of the probes was selected to model basic types of mechanical interactions that we would expect when working on the surface of cosmic bodies such as asteroids. The basic geometry of the probes will result in data that can be extrapolated to more-complex interactions. Later experiments with a motor stage apparatus in vacuum will closely replicate a space environment. During the space-simulated experiments, trials will also include varied amounts of water ice added to the regolith reference surface material. The regolith simulant will also be highly irradiated with UV radiation to account for extreme space environments.

In light of the complexity of the future in-vacuum system, a main goal of the prototype system is to isolate the most important design features for the in-vacuum system, while also acquiring general force trends for each interaction. Results from experimenting with the prototype system will allow us to make helpful design recommendations not only for the Colorado School of Mines in-vacuum system, but for anyone designing a mechanical system that interacts with regolith surfaces. Beneficial parties include not only scientists, but anyone who wishes to conduct space mining activities or create human colonies in space.

2 Background

Many nations and private companies have been expanding the realm of human space exploration, providing economic and technological incentive for future space resource mining of NEOs. As we continue to use precious resources at a nonrenewable rate, the natural inclination is to look beyond Earth to extract these resources. Self-sustaining colonization of space also depends on our ability to extract resources on site, since launching resources from Earth comes at a high cost. Deep Space Industries and Planetary Resources Inc. are two examples of forerunners in the field of space-mining; the latter has partnered with NASA to develop software capable of identifying which asteroids are likely candidates for scientific studies or mineral prospecting [1]. Regrettably, there are few credible sources of experimental data to support the design and development of NEO mining spacecraft. However, some past missions and academic studies provide insight to this endeavor; for example, it is well known that cohesive van der Waals forces between small molecules play a larger role in holding asteroids together than gravitational and centripetal forces [2].

One widely foreseen challenge in developing systems to extract resources from NEOs is the difficulty of anchoring a spacecraft to a quickly moving, oddly shaped, rotating body such as an asteroid. The diverse (and often unknown) types of surface conditions on NEOs further complicate the matter. However, multiple anchoring systems for spacecraft have been modeled, and some even incorporated onto space-bound landers. One anchor model currently in use is on the Philae lander of the Rosetta mission [3]. In November of 2014, Philae became the first spacecraft to make a soft landing on the surface of a comet nucleus, although the landing did not go as smoothly as planned.

The anchoring system of the Philae lander is a combination of harpoons and ice screws. The system was designed so that initial attachment of the lander to the comet surface would be made by the impact energy driving the ice screws into the surface. Upon touch-down, the harpoons were supposed to simultaneously release and penetrate up to 2.5 m into the comet surface. Immediately after being fired, the cable would tighten to 30 N in a period of 8 s, firmly anchoring the lander to the comet nucleus [3]. However, when the lander actually made contact with the comet surface, the initial impact was softer than expected—indicating that the ice screws must not have been driven far enough into the ice to hold the lander in place—and the harpoons and recoil thrusters failed to fire [4]. The combination of these problems caused the lander to bounce twice before finally landing, and during the first bounce it nearly reached the escape velocity of the comet’s low gravity, which would have been disastrous to the Rosetta mission [5]. The landing problems faced during the Rosetta mission are a good example of the complexity of mechanical interactions with NEO surfaces, which is why the CSM team is studying and modifying past designs such as the Philae lander in order to develop and test more successful NEO anchoring systems.

The effectiveness of different anchors can be more clearly characterized when we better understand the physical interactions of regolith particles. Regolith properties can be estimated on Earth by using granular regolith simulants, but more accurate data can be acquired from testing real regolith in space. Rozitis and colleagues discuss how asteroid (29075) 1950 DA was found to have a cohesive strength of at least 64 Pa in the regolith [6]. That asteroid cohesive strength is much less than that of silt (75 kPa) or soft clay

(48-96 kPa) on Earth [7]. Dry cohesion is due to van der Waals forces between regolith molecules. Rozitis and his colleagues also verified that cohesive strength is constant independent of asteroid size. That independence shows that effective models can be scaled down for experiments on Earth without compromising the cohesive strength of a typical asteroid.

Along with anchoring, shearing of regolith is another main area of study for the CSM team working on the IMPACT program. Shearing tools are essential for various types of mineral and resource extraction, yet the fundamental physical properties of regolith under shearing conditions are poorly understood. However, comparisons can be made from similar studies with wedge-like probes that are used in a horizontal shearing fashion. With that intent, the CSM team is using a wedge-shaped probe in a shearing method in order to extract and analyze regolith, resembling a simple horizontal translation of granular particles. This method of extraction can be compared to 'scraping.' The horizontal force resultant on both the surface incident edge and submerged edge of the probe must be analyzed to validate the viability of this type of regolith movement. Also, many studies discuss the high abrasive quality of regolith, so the material of the wedge-tipped probe must be analyzed for durability [8].

The geometry of a wedge probe must be taken carefully into account. For instance, comminution—reducing the size of the particles being mined—must be avoided with this form of probe. Another concern is that wedge interactions might create large reaction forces in other parts of the spacecraft, such as its anchors, which could jeopardize a mission. Unwanted reaction forces can be avoided by knowing that when regolith aggregates, it forms what are called agglutinates [9]. Forces are increased by 'scraping' the agglutinates that are too large, because they generally have stronger interactions with each other. One method to better measure and/or avoid comminution involves using a sensor that can detect when there is too much reaction force on the tip of the wedge. Another method that has been suggested is called a 'controlled fragmentation' [10]. Controlled fragmentation is just a fancy way of saying a controlled explosion near the drill site. When considering this method, it is important to consider how long the effect of the explosion will last. Regolith not only strongly interacts with itself when static, but it also quickly reaggregates after being disturbed.

Several other probe-like experiments on lunar soil have been conducted in the past using a penetrometer. During the 1970's, the U.S.S.R unmanned roving vehicles Lunokhod 1 and 2 traversed a combined 47 km on the lunar surface. During this time, the vehicles performed approximately 1000 cone penetrometer tests to depth of 10 cm. This data was later correlated with measurements taken from lunar samples from Luna 16 and Luna 20, deducing that the lunar surface has an average bulk density of around 1.5 g/cm^3 [11]. A conical-tipped probe replicating a penetrometer is arguably the most basic interaction with a regolith surface, so it will also be used by the CSM team in this project. In the CSM apparatus, the conical-tipped probe will do a simple vertical penetration into the JSC-1A surface.

Since the CSM experiment analyzes basic probe geometries, various types of mechanical interactions, general regolith properties, and a broad range of environments, it will result in data that can be extrapolated to more complex systems. The role of our CSM

team as part of the NASA IMPACT program was to build a prototype motor stage and probes that could be used for preliminary experiments of mechanical interactions with JSC-1A at Earth's atmosphere. After acquiring general force trends for each probe interaction and testing the prototype motor stage, we are able to make credible recommendations for the design of the more advanced in-vacuum apparatus. The force trend data we have already gathered will eventually be combined with that of the in-vacuum system in order to develop a usable database that can support any future endeavors to study or attempt physical interactions with NEOs. The database will provide an overview of credible, repeatable data to the small existing knowledge base of physical interactions with NEO surfaces in space. Therefore, anyone designing a mechanical system to interact with regolith surfaces will benefit from these experiments.

3 Experimental Apparatus, Model and Procedures

3.1 Experimental Apparatus

The apparatus used to perform these experiments consists of two translation stages, both controlled by PM Servo Motors. The horizontal stage is mounted to the carriage of the vertical stage. There is a force transducer mounted to the carriage of the horizontal translation stage. The probe is then mounted to the transducer. A diagram of the set-up is shown in figure 1. The PM servo motors are controlled by Copley motion controllers. The Copleys control the motors by following preset commands according to code written in LabVIEW, thus making the experimental apparatus fully automated. Automation of the apparatus allows easy experimental variation and repeatability of trials.

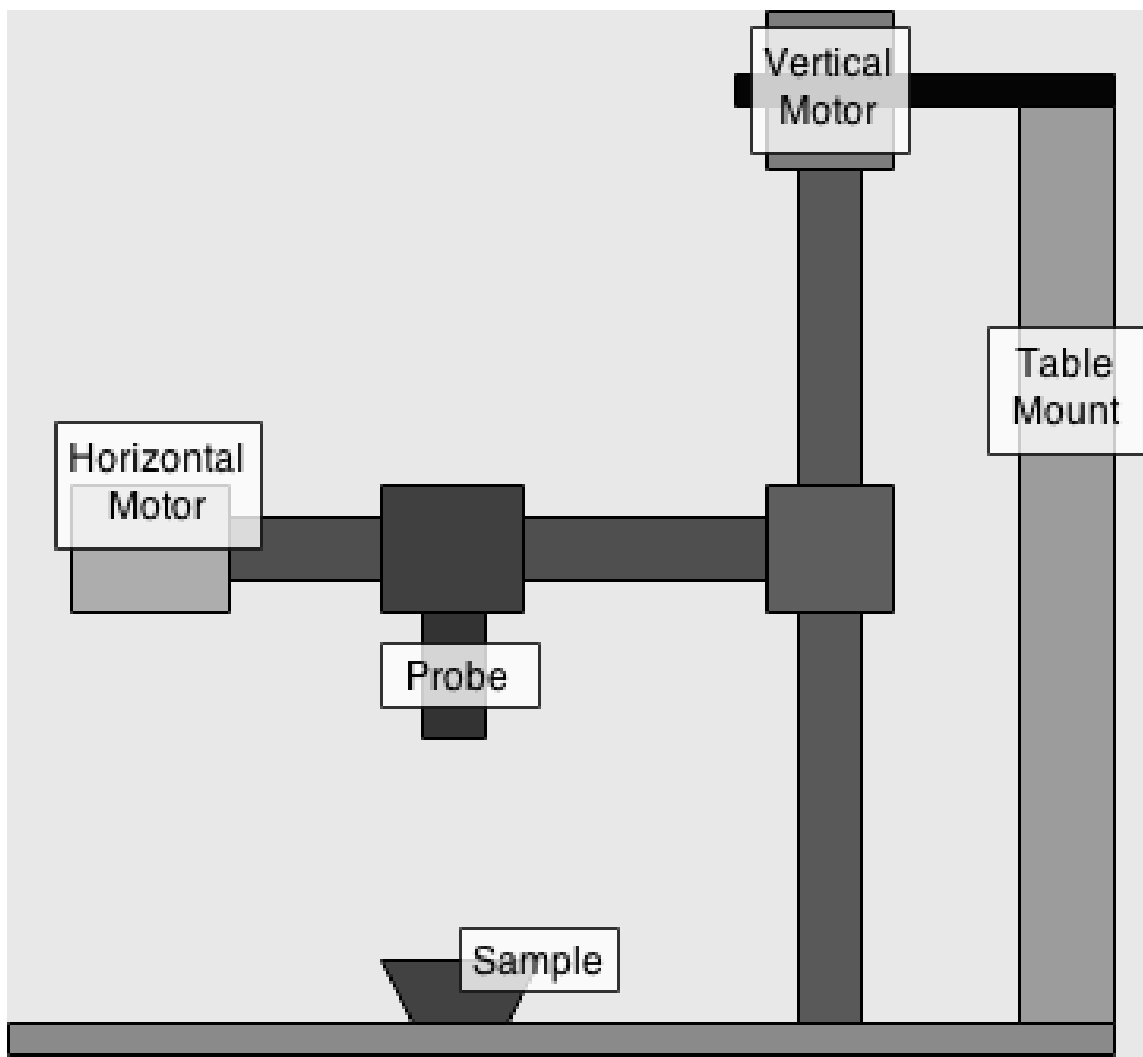


Figure 1: Simple diagram of the experimental apparatus. The supporting electronic equipment such as motor controllers and supporting software are omitted.

4 Experimental Model

The model makes the assumption that the probe is acting as a stiff beam securely attached to the transducer surface. The probes are much stronger than the forces exerted on them by the soil, and the probes are secured flush to the transducer so the assumptions are reasonable. Furthermore, it is assumed (for all probe and experimental variations) that the forces acting on the tip of the probe can be consolidated into a single point force and point moment acting at the very center of the probe as seen in figure (2).

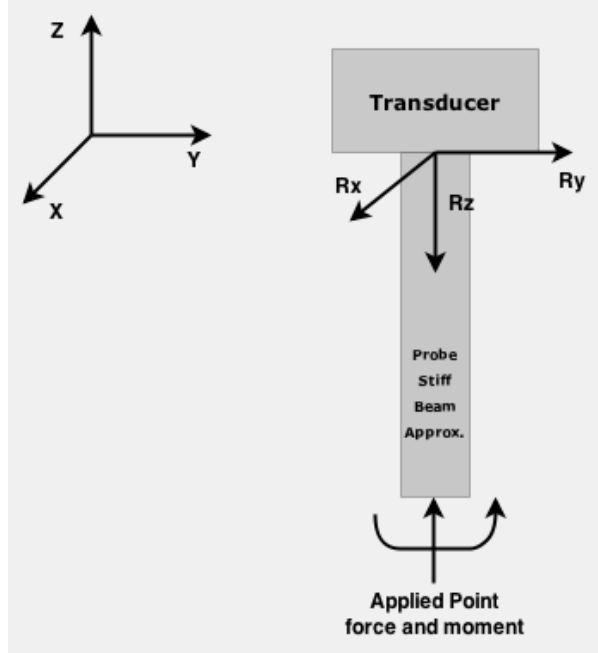


Figure 2: Reference diagram for experimental model. The probe is modeled as a stiff beam centered along the vertical axis. The force on the probe from the JSC-1A is assumed to be a point force and moment applied directly at the tip of the probe and centered on the z-axis.

The stiff beam assumptions are necessary because the transducer reads reaction forces at the point where it connects with the probe, not at the opposite end of the probe where the interactions actually occur. Modeling the probe as a stiff beam allows us to directly relate the transducer/probe interface with the bottom tip of the probe and estimate what forces are present there. Our calculations were performed with the following equations:

$$R_1 = -F_x \quad (1)$$

$$R_2 = -F_y \quad (2)$$

$$R_3 = -F_z \quad (3)$$

$$T_x = (F_z \times R_y) - (F_y \times R_z) \quad (4)$$

$$T_y = (F_x \times R_z) - (F_z \times R_x) \quad (5)$$

$$T_z = (F_y \times R_x) - (F_x \times R_y) \quad (6)$$

Where R_1, R_2, R_3 are the forces in each axis acting on the probe, F_x, F_y, F_z are the forces measured by the transducer, R_x, R_y, R_z are the torque arms and T_x, T_y, T_z are the true torque values.

The torque arms have a dependency on any angles that are created due to the probe being misaligned from the vertical axis. This dependency is shown in equation (7) for the torque arm R , given in vector format and converted to spherical coordinates.

$$R = L < \sin(\theta) \cos(\phi), \sin(\theta) \sin(\phi), \cos(\theta) > \quad (7)$$

Where L represents the length of the beam, which in practice is the distance from the tip of the probe to the measuring surface of the transducer. Using the above relations, the readings from the transducer are converted to forces and torque values acting on the tip of probe.

4.1 Conical Probe Parameters and Procedures

The conical probe is a stainless steel cylinder with a conical tip. The conical tip is tapered at a 30° angle with a 6 mm diameter. The JSC-1A sample container consists of a stainless steel hemisphere with a diameter of two inches. The bowl was chosen to be much larger than the probe so that any forces resulting from the wall of the container pushing back against displaced regolith would be negligible. The interaction that was chosen to be performed with the conical probe is a simple vertical penetration into the JSC-1A surface. This interaction was chosen because it is analogous to cone penetrometer tools or any simple interaction where there is a vertical penetration like that which may occur with various equipment used on comets or regolith terrains. The experimental procedure for the conical probe are as follows:

1. Probe is secured and aligned on translation stage
2. LabVIEW code is initiated
3. Probe moves to home position
4. Probe moves at preset velocity toward sample as data acquisition begins
5. Probe drives into JSC-1A sample until the probe has penetrated to a depth equal to the length of the conical tip section
6. Probe waits 5 seconds
7. Probe is removed vertically from the sample

For consistency the samples were also prepared in a specified manner. Hand pour samples were prepared by pouring a softly mixed volume of JSC-1A roughly equal to the volume of the sample container. The samples were prepared just before running the experiment to ensure that the sample would not settle. The excess JSC-1A was then leveled off using a straight edge. Compacted samples were prepared using the same procedure except for one extra step. After the sample was poured, the bowl was then tamped ten times so the excess sample material settled into the container. The sample was then leveled off just as the hand poured samples are.

4.2 Wedge Probe Procedure

The design of the wedge probe was simple. A 1 cm \times 1 cm \times 3 cm aluminum block would serve as the probe tip. This block was tapped and threaded on the top face. A threaded rod then connected the threaded block to a drill chuck that was mounted to the transducer. This design is susceptible to error if the forces are large enough to cause displacement in the threaded rod's connection to the probe tip. Machining the drill chuck connection and probe tip as a single piece would eliminate this issue in the future. Samples were prepared in a rectangular dish. JSC-1A was poured into the dish until the depth of the soil was 15 mm. The container was then covered and repeatedly dropped in order to create a uniform soil depth, though this method still left inconsistencies. A vibration-compaction method is recommended, and is viewed as the optimal method for creating a uniform soil consistency.

1. Probe is secured and aligned on translation stage.
2. LabVIEW code is initiated.
3. Probe moves to home position.
4. Probe moves at preset velocity toward sample as data acquisition begins.
5. Probe drives into soil until the probe has reached the user-defined penetration depth.
6. Probe waits for 2 seconds.
7. Probe translates horizontally at user-defined velocity until the probe has reached the designated translation distance.
8. Probe waits for 2 seconds.
9. Probe moves to home position.
10. Motors are disabled.

The first motion of the wedge probe was in the negative Z direction to the user-specified penetration depth, somewhere between 5-9 millimeters. The wedge probe entered the JSC-1A vertically at a speed of 7.5 mm/s. Data acquisition began as soon as the wedge probe left the home position. Once it reached the desired penetration depth, the probe halted for two seconds, and then began translating in the positive X direction at a rate of 0.5 mm/s. After the horizontal translation, the transducer stopped recording data, and the stage returned to its home position, and the motors were disabled.

4.3 Anchor Probe Procedure

Originally, the anchor trials were prepared in the same 1.5 inch diameter metal hemisphere used in some of the conical probe trials. However, the anchor went into the sample much deeper than the conical probe, and analysis of the results showed very high (tens of Newtons) and irregular force fluctuations near the end of the trials. We assumed these fluctuations were due to wall effects, so we then changed the experiment to anchor

into a larger container. The latter container is shaped like a cup with a 3 inch diameter and 1.5 inches deep. The strange effects we saw previously were dramatically reduced in the new trials, so we believe that most (though possibly not all) wall effects were removed from the experiment. Additionally, the JSC-1A for these trials was always prepared by light shaking to level the height of the regolith surface, so all trials can be considered as low-compaction trials.

The anchor probe trials required a different mount on the transducer than the other trials because this mount had to also hold the stepper motor that rotated the anchor. The stepper mount was attached to the transducer with four threaded rods, tightened with nuts below the stepper mount as shown below in Figure 3. As will be discussed in our conclusion section, the process of reattaching this mount produced some problems with consistent alignment for trials.



Figure 3: Photo of anchor entering regolith surface during preliminary test trial. Note - In later trials, a larger cup-shaped container replaced the metal hemisphere shown in an attempt to eliminate wall effects.

As with the other experiments, the motors first moved the stage to its preset home position. Next, when the user pressed the "begin trial" button in LabVIEW, several things happened: the force transducer began to record force, position, and velocity data; the vertical motor enabled and began translating the anchor down towards the JSC-1A; and the stepper motor also initiated and began to rotate the anchor.

The anchor rotation speed and vertical translation speed were carefully calculated using the pitch of the anchor to ensure minimal disruption of the JSC-1A as the anchor entered the sample. This is very important because a good anchoring system needs to enter the regolith with minimal disruption so that cohesive strength of the regolith is maintained, allowing the anchor to stay in place with its maximum possible anchoring

force. We chose a slow downward translation velocity of 1.5 mm/s, and we theoretically calculated the matching rotation speed to be 3.515 rev/s. This was a simple calculation as shown below.

$$\frac{R}{P} \times H = R_t \quad (8)$$

Equation 1 gives the number of revolutions that the anchor should experience over its vertical translation distance based on the revolutions and pitch of the anchor flights. R is the number of flight revolutions in the anchor design (9.375 revs), P is the pitch of the anchor (4 mm), and H is the vertical height that the probe is descending while it rotates (35 mm). R_t is the total number of revolutions that the probe should rotate, in this case amounting to 2.344 revs.

$$\frac{H}{S} = T \quad (9)$$

Equation 2 gives the amount of seconds that the anchor should be rotating in order to match the vertical translation speed. H=35 mm (height probe is descending), S = 1.5 mm/s (vertical descent speed), and T = 23 seconds (the amount of time the anchor will be rotating).

Lastly, dividing equation 1 by equation 2 would give us the necessary revolutions per second. This is shown in equation 3 where w is revolutions per second.

$$\frac{R_t}{T} = w \quad (10)$$

During experiments, we found that varying the rotational velocity had interesting effects on the results. In order to attempt to find the perfect experimental rotational velocity for maximum anchoring force (with minimal disturbance of the regolith upon entry) we ran trials at multiple rotational velocities (as shown in the data section of this paper).

For each trial, the bottom tip of the anchor slowly entered the JSC-1A surface at a distance of 13 mm from its home position. Next, both the vertical servo and the rotational stepper motor disabled at the exact time once the anchor had descended the total height of 35 mm, placing the bottom tip of the anchor about 22 mm below the surface of the sample. The program then waits approximately 14 seconds, after which the vertical servo enables again and lifts the anchor out of the sample (again at 1.5 mm/s, and this time with the stepper motor inactive so the anchor is not rotating).

We should also note that original trials were taken with only a two second delay when the anchor was fully inserted into the sample; however, the data showed a seemingly exponential decrease in positive force on the anchor during that time interval, so we decided to increase it to 14 seconds to watch the entire phenomena that was occurring. Further discussion of the exponential decrease in force is present in the data analysis section. Lastly, when the probe returns to its home position, the servo motor is again disabled and data acquisition ends. A diagram of the anchor probe design is shown below.

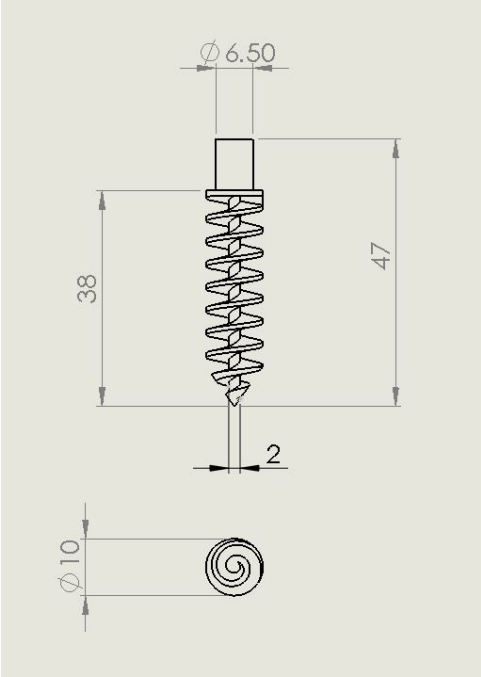


Figure 4: Schematic of anchor design with labeled dimensions. Units are in millimeters.

5 Data and Analysis

Data was acquired at a sampling rate of 1 kHz for all wedge and anchor trials while all conical trials were ran at 10kHz by an ATI Gamma 6-axis transducer, which ran during the entire mechanical movement of each trial, so that data was acquired both before and after physical interaction of the probe with the JSC-1A. Data was then trimmed and converted in MATLAB to yield force versus position relationships. The raw data read by the transducer was transformed into force data on the probe using the experimental modeling equations, and then filtered using standard 1st order low pass filtering techniques. All data has uncertainty values corresponding to table 2 (see error analysis section for explanation). All plots and data analysis shown below are created using MATLAB.

5.1 Force Trend Data

5.1.1 Conical Probe

The conical data is only concerned with the vertical (z-axis) of the probe. This is due to the fact that the conical probe trials were performed using only the vertical axis. Also, The conical probes and sample container are symmetrical about the vertical axis. Therefore there are no significant torques on any axis, and there are no significant forces acting on the probes about any axis other than the vertical (z-axis) axis. Figure (5) below shows the force data for a "hand poured" trial while figure(26) shows an example of a "compacted" trial. All conical trial data was sampled at rate of 10kHz and the probes moved at a velocity of $2.5\frac{mm}{s}$, giving the conical data an effective resolution of $4000\frac{datapoints}{mm}$.

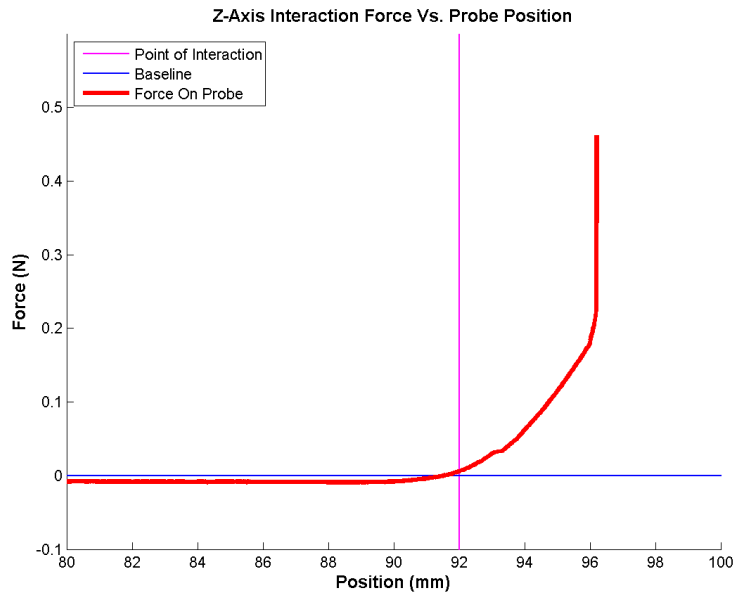


Figure 5: Compacted Trial 1: Vertical Force(N) Vs. Position (mm) of probe using a 6mm diameter probe on a compacted sample poured sample. The point of interaction line denotes where the probe first comes into contact with the simulant surface and the baseline is the 0 force axis. The position is based off of an absolute distance from the starting position of the probe. This trial hits a max force value of 0.46 ± 0.043 N

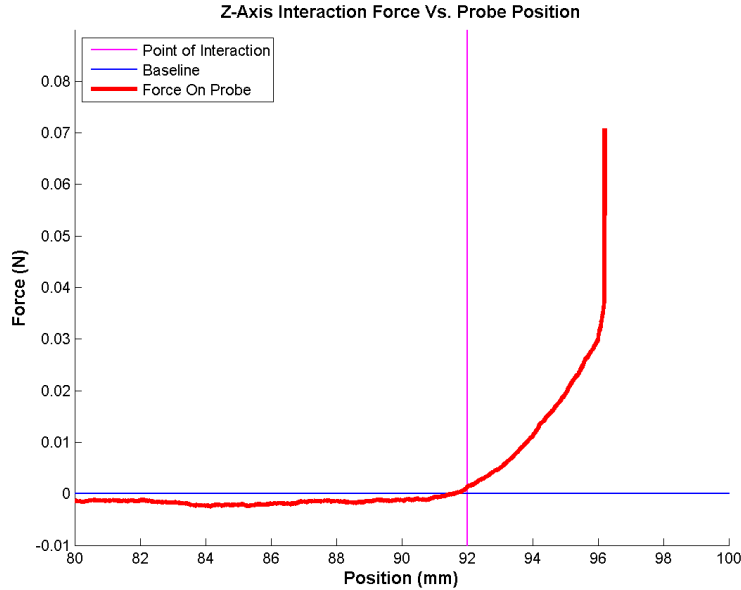


Figure 6: Poured Trial 1: Vertical Force(N) Vs. Position (mm) of probe using a 6mm diameter probe on a hand compacted sample. The point of interaction line denotes where the probe first comes into contact with the simulant surface and the baseline is the 0 force axis. The position is based off of an absolute distance from the starting position of the probe. This trial hits a max force value of 0.071 ± 0.043 N

As can be seen in figures 5 & 6 above, the conical trials have a very simple upward slope that steadily increases as the probe enters the surface followed by a sharp climb in force value as the probe stops penetrating the JSC-1A. This overall trend models what would be expected for a conical cone tipped probe. As the probe is penetrating, more and more of the probes conical surface area comes in contact with the soil and so increased forces are to be expected. Also during this time, simulant material is being displaced away from the probe surface. The displacement of the soil can create pressure and potentially compact the soil under and around the probe. This behavior could help to explain the sharp rise in force when the probe reaches its maximum penetration dept, the soil stops being displaced and instead pushes against the probe in a more compacted state.

Another important aspect of the conical probe trials is the difference in force values between the hand poured and compacted samples. The two trials above for example have max force values of 0.46 ± 0.043 N for the compacted sample and 0.071 ± 0.043 N for the poured sample showing a whole magnitude of difference. Taking average peak force values for each type of trial showed that the compacted force values were on average 5.7 times greater than the hand pour trials. This is an expected result since it has been shown that JSC-1A is best compacted by means of mechanical vibration similar how these samples were prepared[13]. The values for peak force on the probe for all four of the trials can be seen below in table 1.

It is also worth mentioning how the force trend line tends to dip below the 0 force baseline. The graphs can be deceiving, leading one to believe that there is serious error in the results. However, since the forces that are being measured are very small in nature, and somewhat similar in magnitude to the uncertainty in the transducer, and since the

Trial	Peak Force (N)
Poured 1	0.071 ± 0.043
Poured 2	0.055 ± 0.043
Compacted 1	0.462 ± 0.043
Compacted 2	0.253 ± 0.043

Table 1: Table of peak force values across all conical probe trials.

LabVIEW code running the apparatus is using a real time biasing calibration, serious error is not necessarily the case. Furthermore, when the probe begins to actually interact with the surface, the forces are big enough in comparison to consider the drift below the 0 force value to be negligible.

5.1.2 Wedge Probe

The force and torque data for the wedge probe trials is plotted in the figures below. Both trials were performed at .5 mm/s. The first trial was run at a penetration depth of 5 mm, the second at a depth of 7 mm. All trials are run following a manual compaction of the regolith simulant. The force from the JSC-1A is separated into horizontal and vertical components, where horizontal means in the direction of motion. The third graph is of the torque about the X axis. A first-order low pass filter with a cut-off frequency of 1000 Hz was used to process the transducer data.

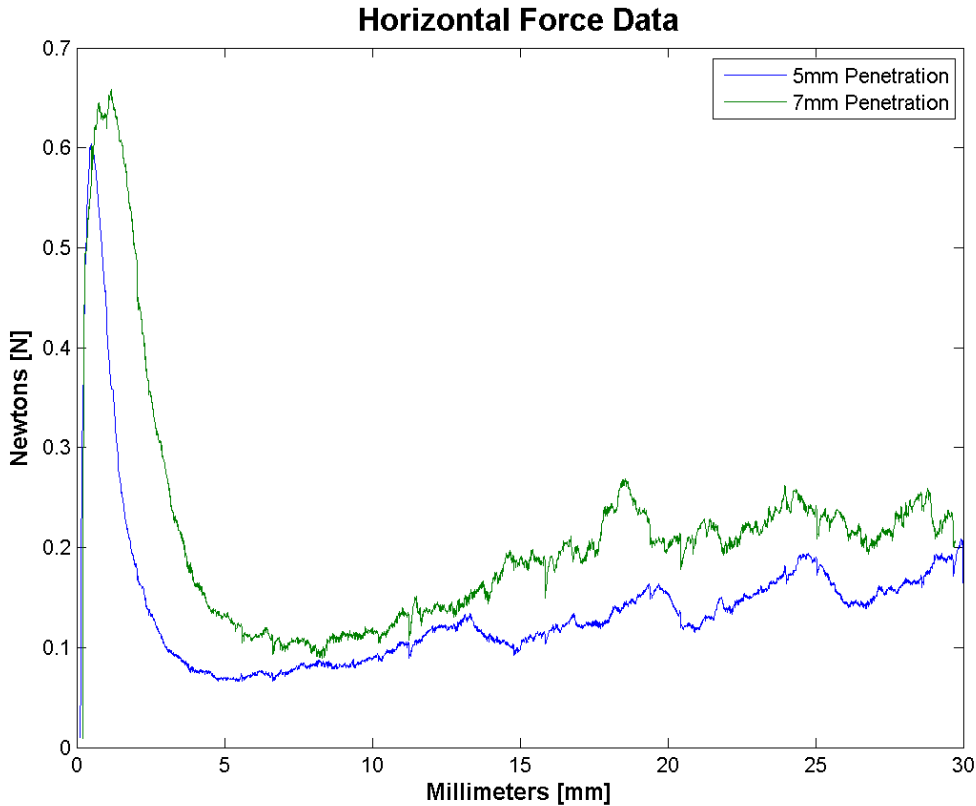


Figure 7: Graph of horizontal force on the transducer for the .5 mm/s trials.

In the horizontal force data we see an initial peak in force as the probe begins trans-

lation. Once the probe is moving, the forces drop, and we start to see smaller waves in the horizontal force values. It is likely that this is due to the build-up and subsequent breaking apart of the particles present directly in front of the probe. We also see a generally upward trend in the force values after the initial drop. This suggests that the breaks that occur later on do not remove as much JSC-1A as is being built up.

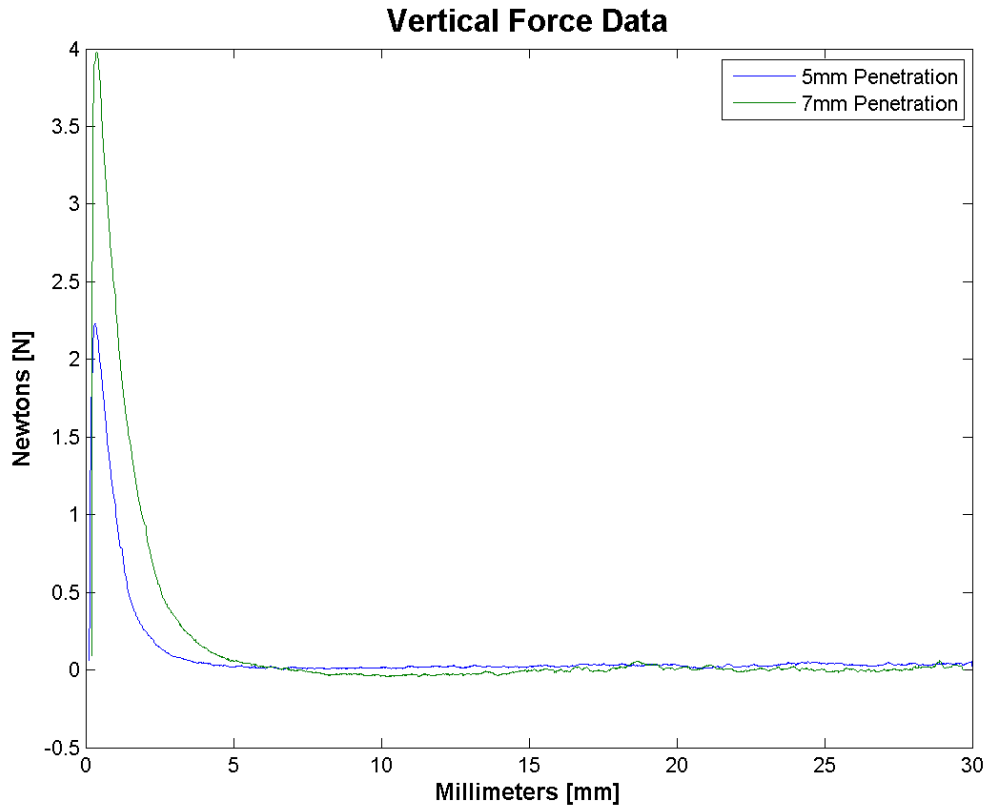


Figure 8: Graph of vertical force on the transducer for the .5 mm/s trials.

It is clear from the vertical force data (figure 8) that there are compaction forces present right at the point of insertion. This makes sense, because as the probe comes down it compacts what is under it. We do not see any compaction forces present once the probe moves away from the point of impact.

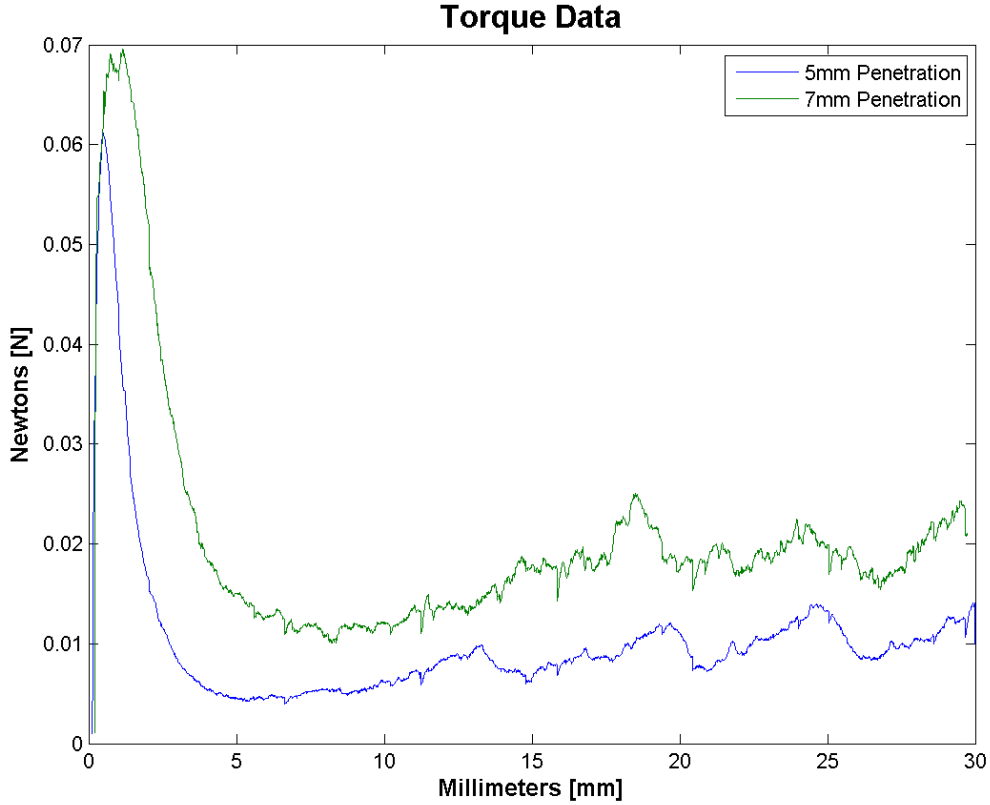


Figure 9: Graph of torque on the transducer for the .5 mm/s trials.

The torque data is strongly correlated to the horizontal force data, which is what we expect in ideal conditions. The probe has a length of .105 meters, so the expected torque about the X-axis from the horizontal force can be found from the simple equation below.

$$T_x = -F_y \times .105 \quad (11)$$

This relationship is very representative of what we see in the plots of the actual data, meaning the correlation between force and moment which our model predicted is accurate for our system. In other words, the data shows that the force at the tip of the probe is being directly translated to the transducer.

Another factor we noticed about the data is the inconsistency of the force values, even among trials with identical parameters. The inconsistencies are likely due to the variable compaction, depth, and relative composition of the JSC-1A in the container. A manual compaction method was used before each of the trials to minimize this effect. A vibration-based compaction would be optimal to reduce this further.

5.1.3 Anchor Probe

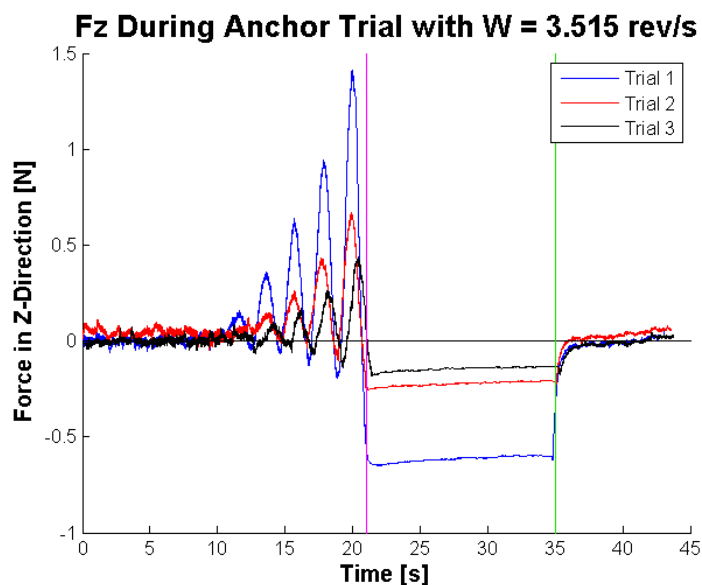


Figure 10: Plot of force in the z-direction over time increment of complete anchor trial with rotational speed $w=3.515$ rev/s. Magenta line marks when anchor probe stops movement and is completely submerged in regolith surface. Green line marks when anchor probe begins ascending from below the regolith surface.

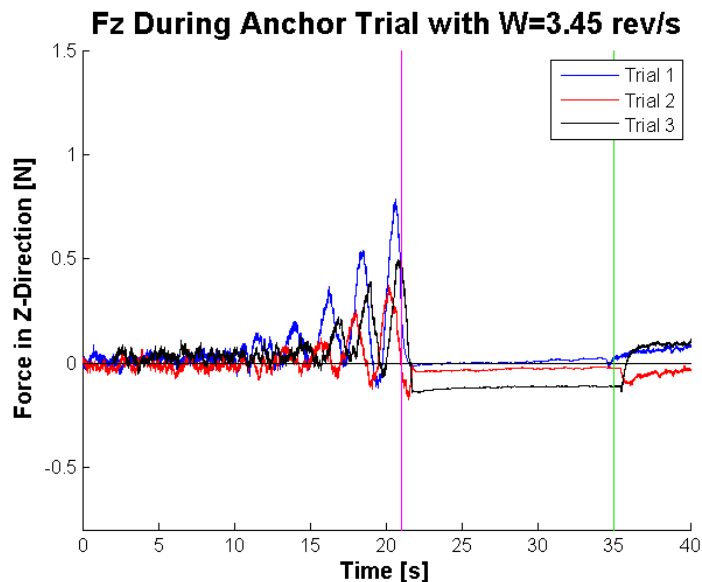


Figure 11: Plot of force in the z-direction over time increment of complete anchor trial with rotational speed $w=3.45$ rev/s. Magenta line marks when anchor probe stops movement and is completely submerged in regolith surface. Green line marks when anchor probe begins ascending from below the regolith surface.

Figures 10 and 11 show the force in the z-direction during complete anchor trials operated at $w = 3.515$ rev/s and $w = 3.45$ rev/s, respectively. The bottom tip of the anchor enters the JSC-1A between 12 and 13 seconds into the trial. Shortly after this, we begin to see

oscillations in F_z of increasing magnitude as the anchor descends into the JSC-1A.

We had hypothesized that if the anchor design and motor control were ideal, then the forces present on the anchor as it entered the regolith surface should be minimal, thus leaving the regolith relatively undisturbed in order to preserve a strong anchoring pull-out force. What we found was a positive Z-direction force (of magnitudes on the scale of tenths of Newtons) pushing back up on the anchor probe as it entered the surface. Unexpected to us, this upward force was oscillating as it increased to its max amplitude. With the current experimental setup, it is difficult to determine whether the oscillations are due to experimental errors such as misalignment of the anchor probe, non-ideal translation or rotational speed, flaws in anchor design/manufacturing, or if the oscillations actually represent natural occurring phenomena during the process of inserting an anchor into a regolith substance. As shown below in Figure 12, we did see that the oscillations were not present when running anchor trials without the probe actually entering any regolith, so we can at least eliminate motor noise from being a factor for the large oscillations.

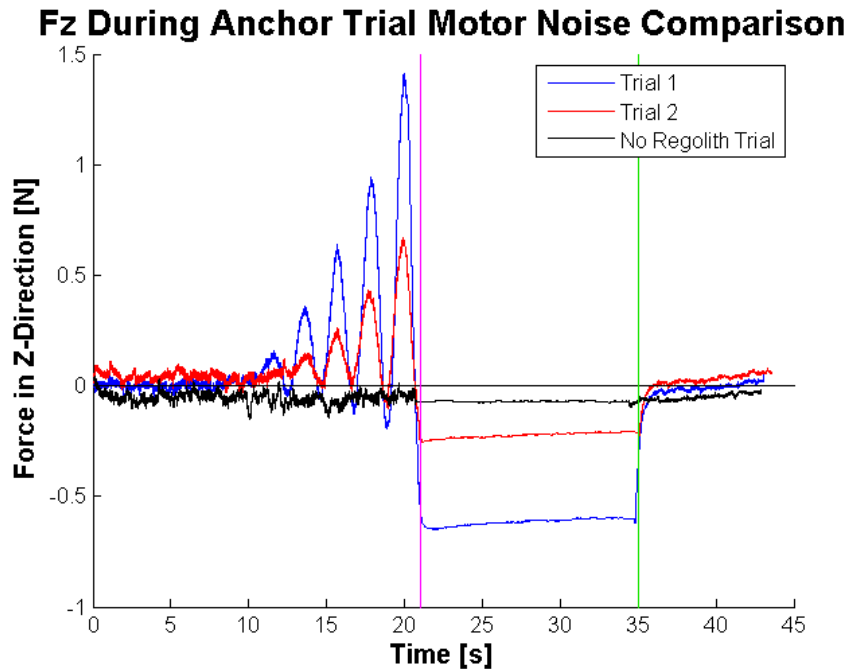


Figure 12: Plot of Force in Z-Direction with with no regolith trial to compare amounts of motor noise

The oscillating force stops at about 21 seconds, at which point the anchor stops both rotating and translating into the JSC-1A (this is marked by the magenta line in Figures 10, 11, and 12). Next, during the 14 seconds that the anchor probe is motionless in the JSC-1A, we see a gradual decrease in the positive z-direction force that lasts roughly seven seconds. The decrease in vertical force appears to trend exponentially until it levels off at a negative force value. This seemingly exponential decrease in positive force on the anchor while it is not moving was also surprising to us. The decrease may be attributed to experimental error in how force was transferred from the tip of our probe to the transducer; however, it may also be due to natural phenomena such as the JSC-1A acting as a viscoelastic material that originally pushed up on the probe, but then gradually relaxed with time. Regrettably, the simplicity of this experimental model does not allow

us complex enough understanding of how the regolith particles around the anchor probe are interacting to draw solid conclusions for this phenomena.

After the anchor sits motionless and submerged in the JSC-1A for about 14 seconds, the anchor begins to pull up vertically out of the regolith as marked by the vertical green line at 35 seconds into the trial. At the moment the anchor begins to be pulled out of the sample, some trials show a sudden increase in negative z -direction force which may account for the actual anchoring force that the probe must overcome to be pulled out of the surface. We expected to see an anchoring pull-out force such as this in the data, though we hypothesized that it would be of higher magnitude than we actually witnessed. It is likely that our anchor is not being controlled ideally to act as an efficient anchor which would not disrupt soil upon entry and would hold firmly during extraction. Regardless, after the small area of pull-out force near the green vertical line, the force then tends to trend positively again until the anchor is pulled completely after the surface.

Once the anchor was out of the regolith, we assumed to see the force come to rest at a level slightly higher than the original baseline force due to the added weight of regolith on the anchor flights. We estimated the volume of empty space on the anchor that gets filled with regolith to be about 6 cm^3 , which gives a weight of about 0.076 Newtons based on the 1.3 g/cm^3 density of low-compacted regolith. The addition of that very small force from the weight of the regolith is difficult to decipher from the plots since it is near the noise range of the stepper motor during the initial baseline weight measurement.

Below are more example plots of the forces present during the trials with $w = 3.515$ rev/s. In the below figures, plots have been split up into descent and ascent of the probe, to show a more detailed relationship between the force and torque components acting on the tip of the probe, versus the position of the probe during the trial.

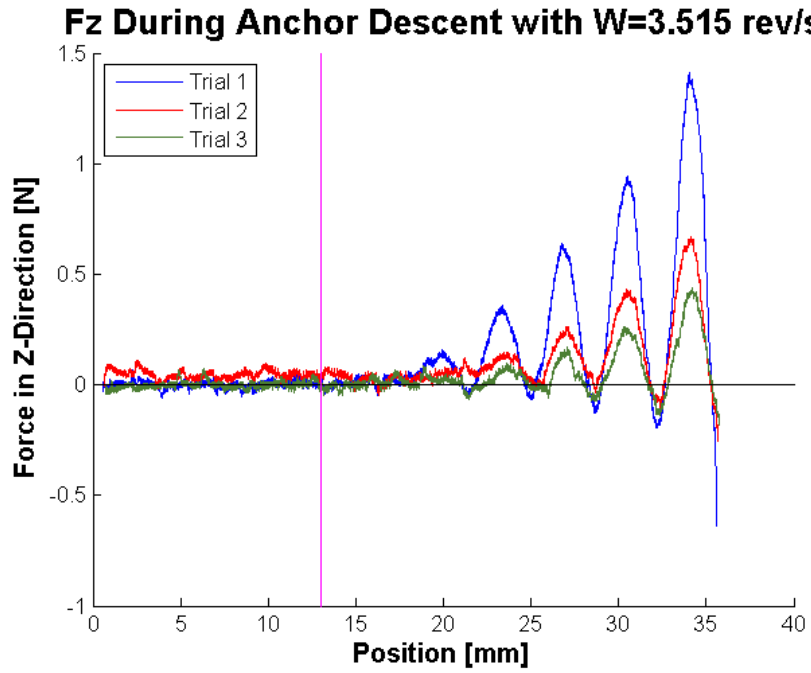


Figure 13: Plot of three separate trials showing force in the Z-Direction during descent of the anchor into regolith sample at $w=3.515$ rev/s. Magenta line marks point when bottom tip of anchor probe first enters the regolith surface.

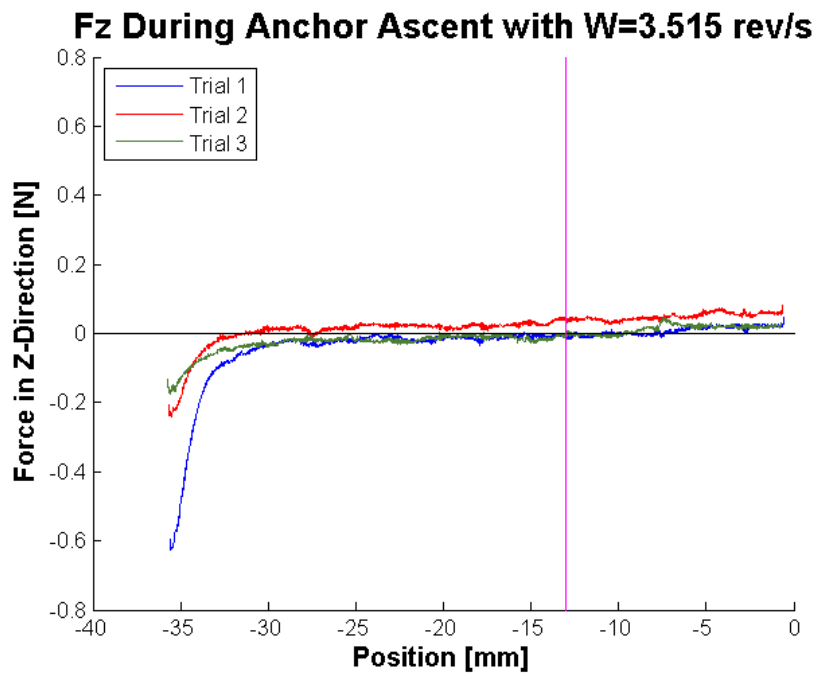


Figure 14: Plot of three separate trials showing force in the Z-Direction during ascent of the anchor out of the regolith sample. Magenta line marks point when bottom tip of anchor probe leaves the regolith surface.

For both descent and ascent of the anchor, the forces in the z-direction (Figures 13 and 14) were the highest measured components of force. We believe that makes sense

with our simple model of the anchor probe as a stiff beam, so z-direction forces should dominate vertical anchor movement. Forces measured in the y-direction are shown below in figures 15 and 16. These F_y forces are of low magnitude, and the trends correspond well with F_x forces which can be viewed in the Appendix.

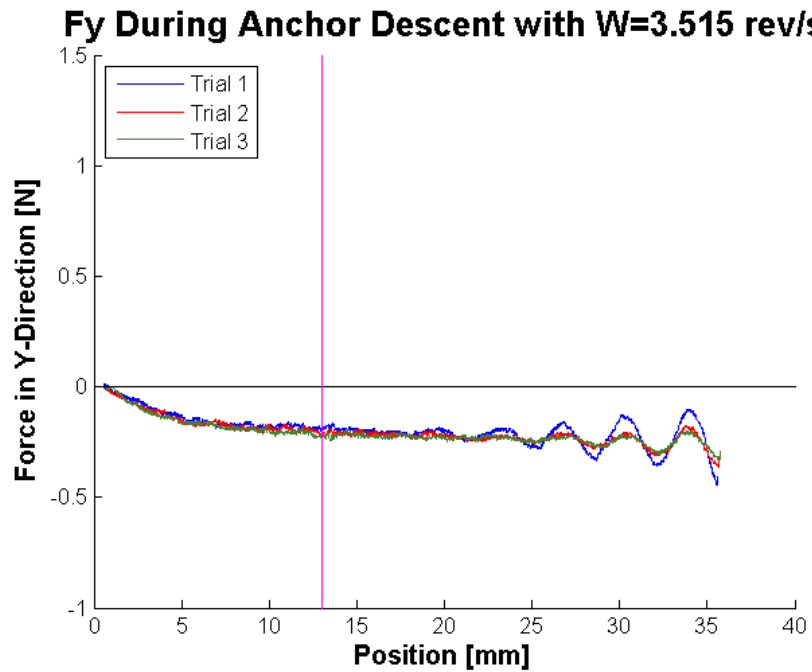


Figure 15: Plot of three separate trials showing force in the Y-Direction during descent of the anchor into the regolith sample with speed $w=3.515$ rev/s. Magenta line marks point when bottom tip of anchor probe first enters the regolith surface.

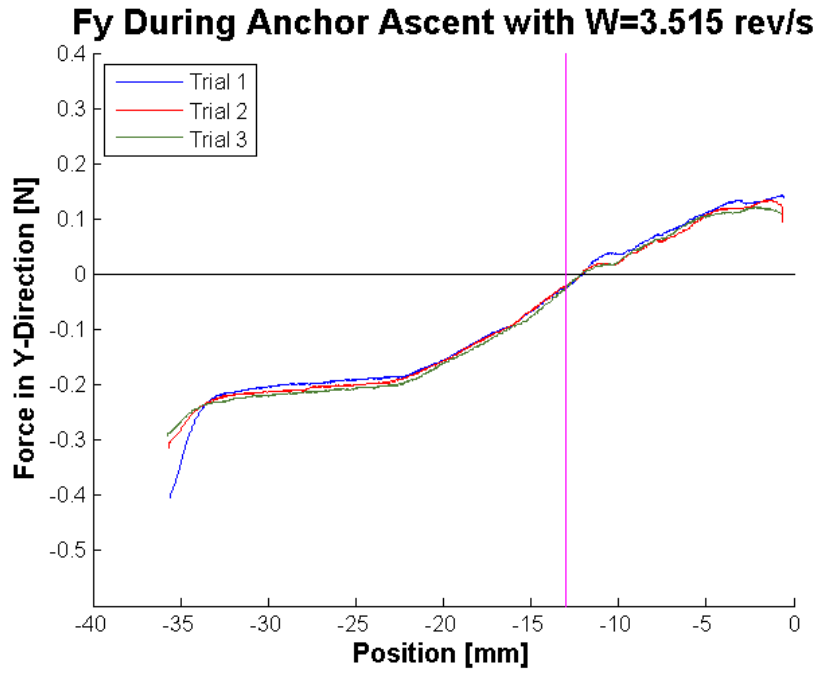


Figure 16: Plot of three separate trials showing force in the Y-Direction during ascent of anchor out of regolith sample. Magenta line marks point when bottom tip of anchor probe leaves the regolith surface.

Lastly, figures 15 and 16 show the corresponding torque about the y-axis during ascent and descent of the anchor. These torques oscillated in magnitude along with the forces that caused them. Again, it is difficult to distinguish if the oscillations are simply due to errors in offset of the probe which could change the directions of the forces as the anchor rotates, or if they are due to some more complex phenomena with particle interaction. Torques about the x and z-axes can also be viewed in the Appendix.

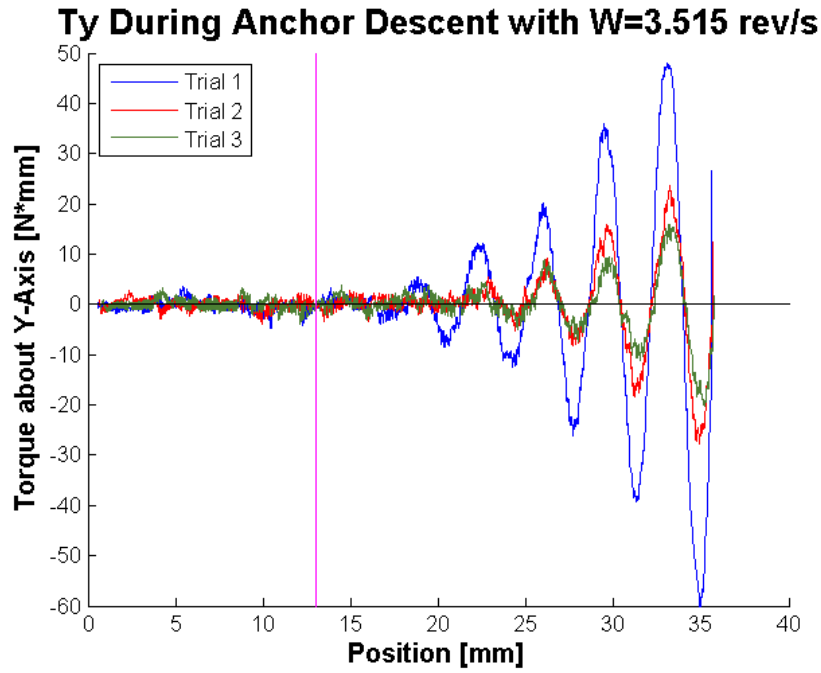


Figure 17: Plot of three separate trials showing torque about Y-axis during descent of anchor into regolith sample at speed $w=3.515$ rev/s. Magenta line marks point when bottom tip of anchor probe first enters the regolith surface.

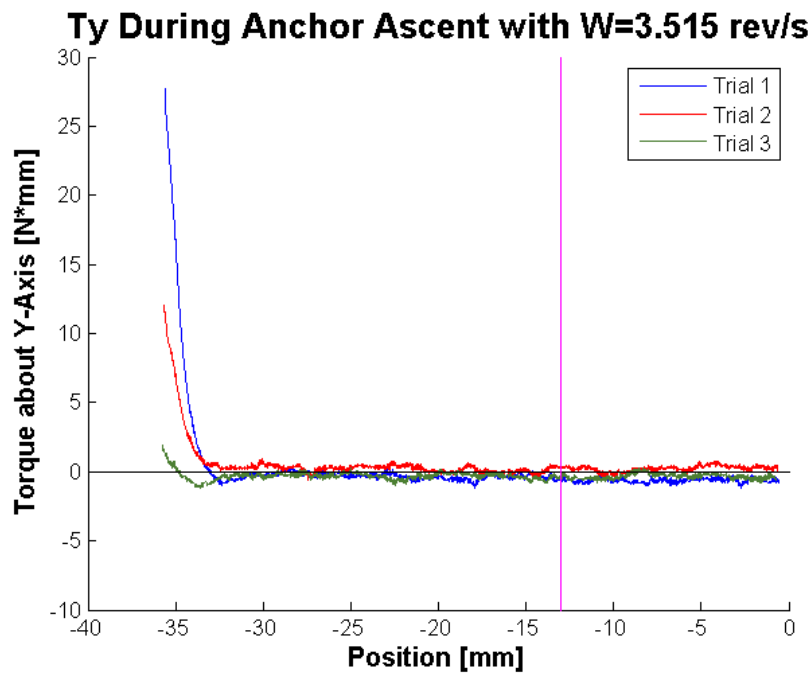


Figure 18: Plot of three separate trials showing torque about Y-axis during ascent of anchor out of regolith sample. Magenta line marks point when bottom tip of anchor probe leaves the regolith surface.

5.2 Error Analysis

There are two sources of error present in the force data for all three types of probe. There is the error due to the accuracy and resolution of the transducer and also errors due to the probe(s) being misaligned along the vertical axis. The transducer comes with an accuracy rating as a part of its calibration certificate. The accuracy ratings are given as percent error of max load value of the transducer. The computed accuracy for each axis/measurement are given in table 2 below:

	Accuracy Error (N)
F_x	0.32
F_y	0.32
F_z	0.20
	Accuracy Error (N-M)
T_x	0.05
T_y	0.05
T_z	0.025
	Uncertainty (N)
F_x, F_y, F_z	0.043
	Uncertainty (N-m)
T_x, T_y, T_z	0.043

Table 2: Accuracy error values and uncertainty ranges of the ATI Gamma transducer used in all experiments.

There errors in accuracy are somewhat large compared to the force values seen across all the experimental trials, which suggest that the absolute value of forces recorded may be quite inaccurate. However it can be reliably said that the relative sizes of forces are precise. This means that the relative size of forces and max force values are still valid measurements. This is due to the very low level of uncertainty and high level of resolution given by the transducer. The uncertainty in transducer measurements was found by taking the standard deviation of data taken during a dry trial with no parts of the apparatus active. The data analyzed was thus the transducer noise and can therefore be used to calculate the uncertainty in transducer measurements. The calculated uncertainty values can be found in table 2.

The second type of error present in the apparatus is due to the probes being misaligned from a perfect center along the vertical z-axis. The entire apparatus was initially leveled and balanced to the point where it became impractical to directly measure the angle of offset with available tools or methods. Therefore, in order to get an estimate of the error in angle offset of the probe from the vertical axis, a simple experiment was carried out for each probe. The simple experiment consisted of applying a known vertical load on the probe. Force and torque readings for all axis were taken using the transducer. Using the experimental model equations, the error in angles were calculated by solving the systems of equations. The error in force values are equal to the transducer uncertainty because they are the only variable that the force values depend on with error. The torque values have a compounded uncertainty resulting from their experimental model

equations. Below is a sample calculation for T_x . All of the errors in torque follow the same method as follows:

Uncertainty was evaluated using the following general equation:

$$S_z = \sqrt{\left(\frac{\partial z}{\partial x}\right)^2 S_x^2 + \left(\frac{\partial z}{\partial y}\right)^2 S_y^2} \quad [14]$$

Applying this equation to the experimental equation for T_x the following expression is obtained:

$$T_x = \sqrt{(F_z * \delta R_y)^2 + (R_y * \delta F_z)^2 + (-R_z * \delta F_y)^2 + (-F_y * \delta R_z)^2}$$

Where δ represents the uncertainty for that variable. δR_z for example expands into:

$$\delta R_z = \sqrt{(\cos \theta * \delta l) + (-l \sin \theta * \delta \theta)}$$

where l represents the length of the torque arm.

As can be seen in the uncertainty equations above, torque has a dependence on the angle at which the probe is offset from the z-axis and also the length of the torque arm and all the measurement uncertainty values. However, the result of these equations when actual uncertainty in measurement values were used revealed that the uncertainty added on top of the transducer uncertainty is negligible. Therefore, all uncertainty values are considered equivalent to the ones listed in table 2. This is not a surprising result considering the small values of uncertainty in measurements of the transducer, offset angles of probes and the uncertainty in probe length. The conical trials for example had uncertainty values of 0.00187 degrees for angle of alignment, and 0.0005 mm for the probe length since a micrometer was used, and this is combined with the small uncertainty values of the transducer readings given in the above table.

6 Cost analysis

A cost analysis for the project is shown below in Table (3). There are very few cost associated with experimental apparatus equipment or sample materials due to the high level at which recycled equipment was used, and the fact that a lot of the work performed was data analysis and calculations done electronically on the computer. Furthermore, Many of the materials not recycled from previous work was readily available in the lab and so was not incorporated into the cost of the analysis. The labor cost was made assuming a constant pay rate of \$12.50 per student, each working six hours a week for the duration of the project.

Cost Analysis				
Item	Unit Cost	Quantity	Unit	Cost
Conical-Tipped Probes	\$10.50	3	ea	\$31.50
1" Hemishpere	\$3.49	1	ea	\$3.49
1.5" Hemisphere	\$4.13	1	ea	\$4.13
2" Hemisphere	\$5.20	1	ea	\$5.20
Flat-Tipped Probes	\$13.50	2	ea	\$27.00
Table-Top Motor Stage Apparatu	\$500	1	ea	\$500
Stepper Motor	\$16	1	ea	\$15.95
Stepper Motor Mount	\$5	1	ea	\$5.00
Labor-3 students	\$12.50	288	hr	\$3,600.00
Overhead (50% of labor)	--	--	--	\$1,800.00
TOTAL COST:				\$5,992.27

Table 3: Preliminary cost analysis table for the "Physical Interaction of Simple Tools with the Surface of Airless Bodies" project .

7 Conclusions

Our experiments with our prototype system enabled us to get an indication for the force trends and magnitudes that we can expect to see in the future when using the in-vacuum system. We were also able to analyze the errors associated with the experimental design, and were able to determine what alterations to the prototype are necessary to facilitate in-vacuum testing.

One of our main focuses in running these experiments was to determine if the prototype translation stage was sufficient for the in-vacuum testing. One major source of error associated with the experiment was the consistency of the sample. Manual compaction techniques are not sufficient for getting uniform sample consistency. This was very noticeable in the wedge probe trials because as the range of motion increased, so did the variations in depth. Vibratory compaction is the optimal compaction method for regolith of this type, and should definitely be used for the more accurate in-vacuum system.

Another aspect of the design that should be altered is the mount for the probes. Having different mounts for each probe meant that alignment was necessary every time the probes were switched. Additionally, the mount for the in-vacuum system should be large enough to house the stepper motor used for the anchor trial, as opposed to an external connection between the mount and the motor as we had in our prototype system. This was by far the biggest issue we had when trying to align the probes.

Furthermore, we recommend that the motors used in the in-vacuum system be tuned carefully to eliminate background noise since the forces being measured are so small. Additional helpful changes could include use of a closed-loop system that allows real-time force-feedback adjustments to ensure the reliability of constant force or constant velocity trials, and force sensors in the regolith itself to allow better understanding of particle interaction.

8 Appendix

8.1 Additional Anchor Probe Plots

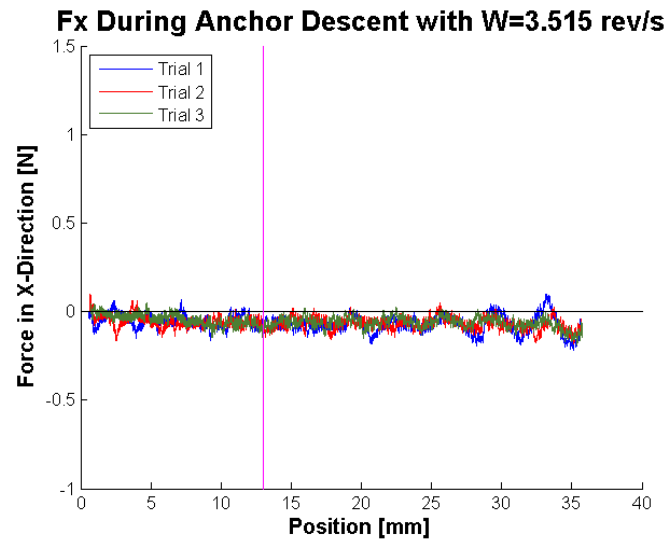


Figure 19: Plot of three separate trials showing force in the X-Direction during descent of the anchor into regolith sample at $w=3.515$ rev/s. Magenta line marks point when bottom tip of anchor probe first enters the regolith surface.

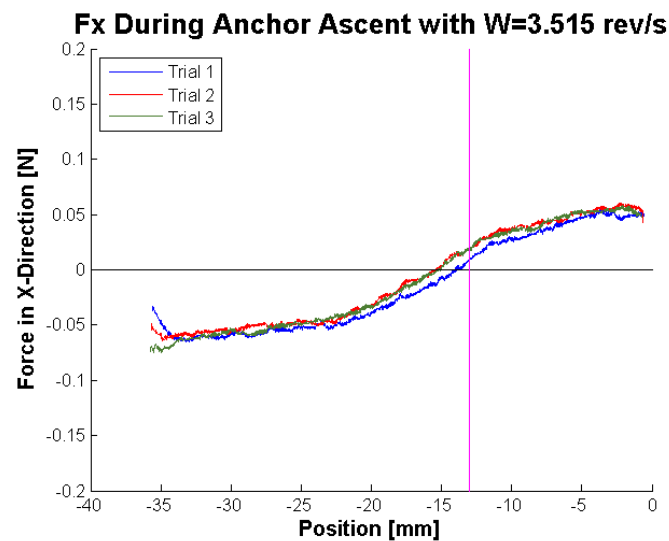


Figure 20: Plot of three separate trials showing force in the X-Direction during ascent of the anchor out of the regolith sample. Magenta line marks point when bottom tip of anchor probe leaves the regolith surface.

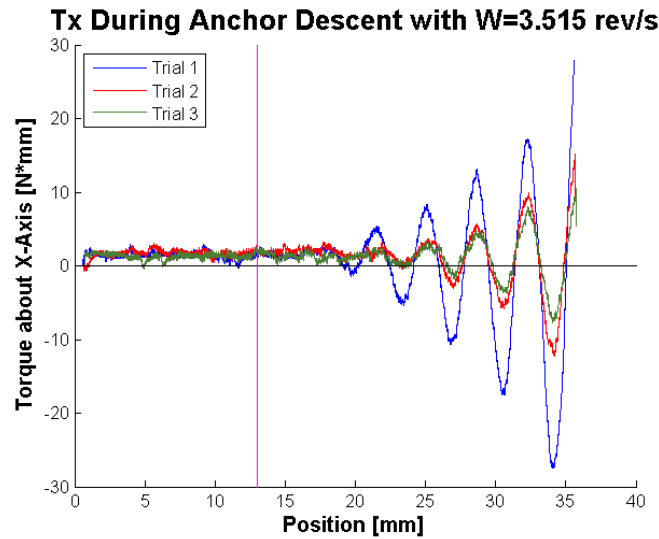


Figure 21: Plot of three separate trials showing torque about X-axis during descent of anchor into regolith sample at speed $w=3.515$ rev/s. Magenta line marks point when bottom tip of anchor probe first enters the regolith surface.

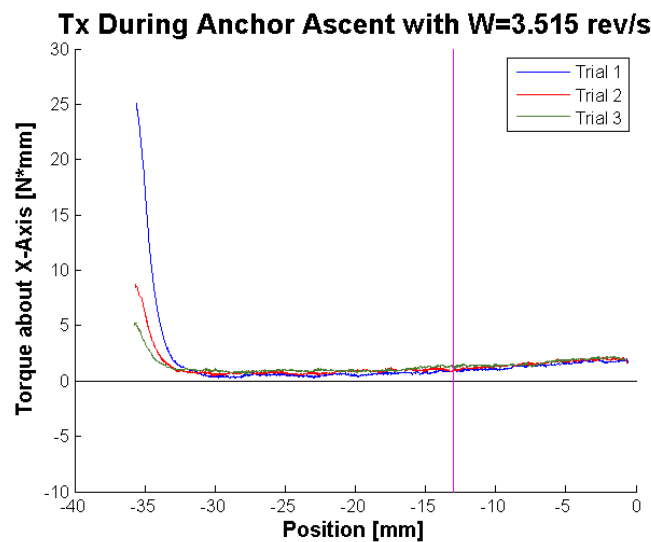


Figure 22: Plot of three separate trials showing torque about X-axis during ascent of anchor out of regolith sample. Magenta line marks point when bottom tip of anchor probe leaves the regolith surface.

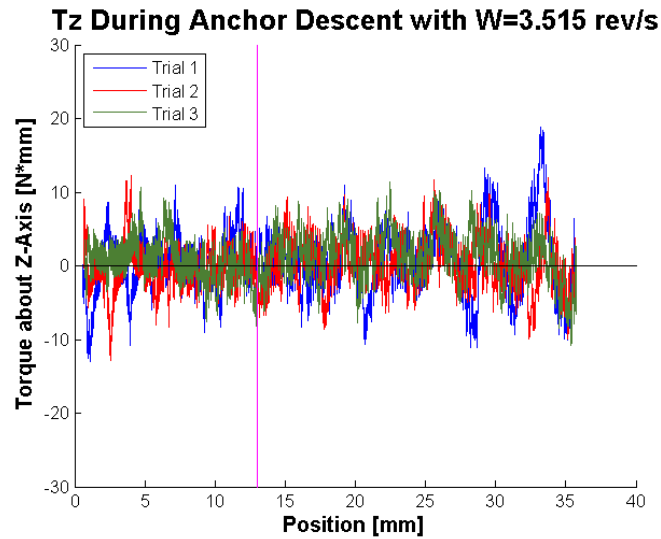


Figure 23: Plot of three separate trials showing torque about Z-axis during descent of anchor into regolith sample at speed $w=3.515$ rev/s. Magenta line marks point when bottom tip of anchor probe first enters the regolith surface.

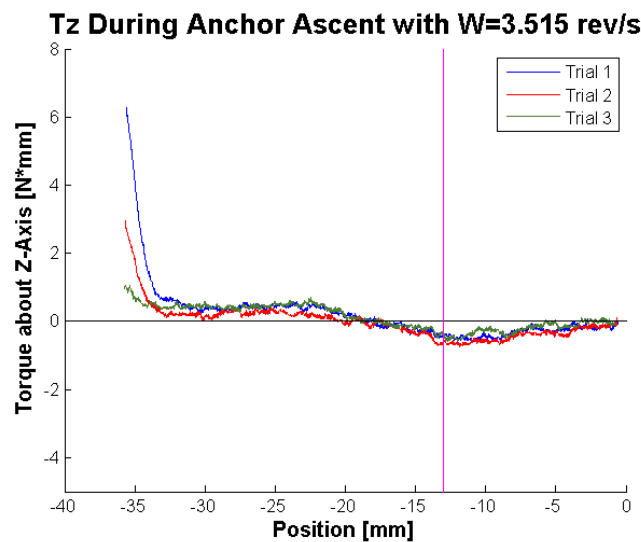


Figure 24: Plot of three separate trials showing torque about Z-axis during ascent of anchor out of regolith sample. Magenta line marks point when bottom tip of anchor probe leaves the regolith surface.

8.2 Additional Conical Probe Plots

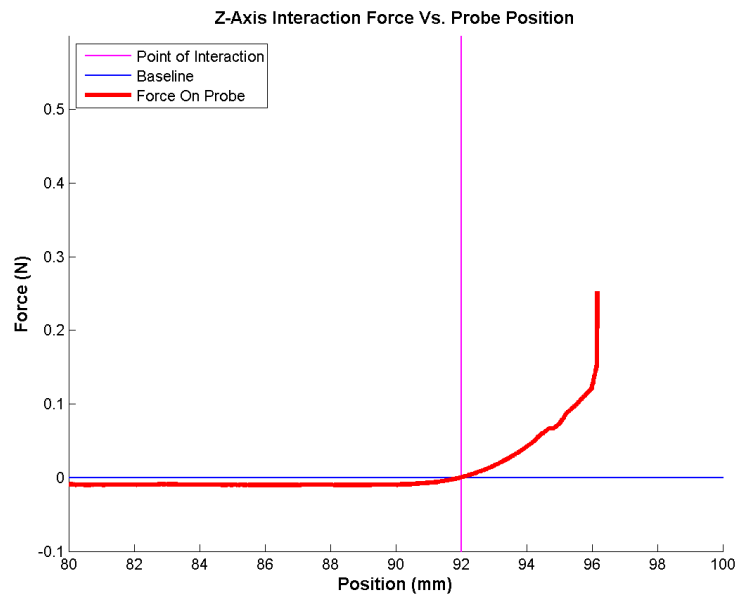


Figure 25: Compacted Trial 2: Vertical Force(N) Vs. Position (mm) of probe using a 6mm diameter probe on a compacted sample poured sample. The point of interaction line denotes where the probe first comes into contact with the simulant surface and the baseline is the 0 force axis. The position is based off of an absolute distance from the starting position of the probe. This trial hits a max force value of 0.232 ± 0.043 N

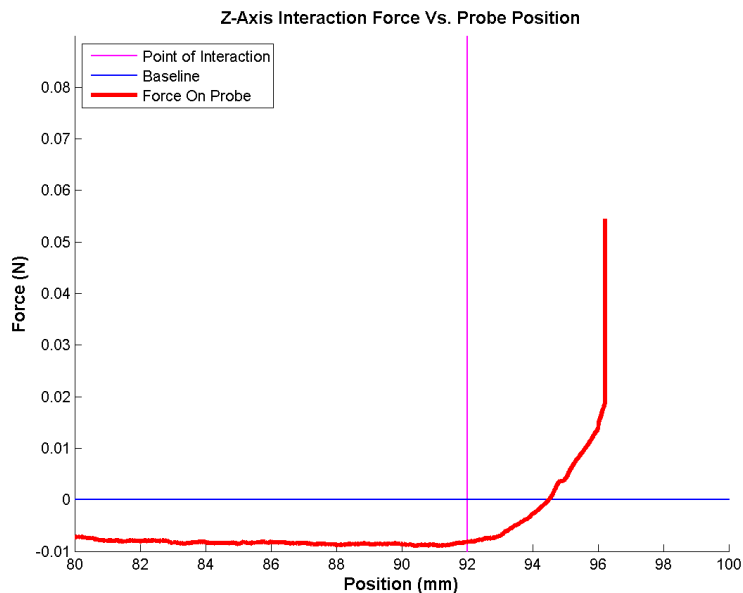


Figure 26: Poured Trial 2: Vertical Force(N) Vs. Position (mm) of probe using a 6mm diameter probe on a hand compacted sample. The point of interaction line denotes where the probe first comes into contact with the simulant surface and the baseline is the 0 force axis. The position is based off of an absolute distance from the starting position of the probe. This trial hits a max force value of 0.055 ± 0.043 N

References

- [1] Megan, Gannon, "NASA teams with asteroid-mining company to crowdsource space rock hunt," <http://www.space.com/23702-nasa-asteroid-detection-crowdsourcing-contest.html> 28 September 2014.
- [2] T.D. Oswalt, "An overview of the Asteroids and Meteorites," *Planets, Stars and Stellar Systems* A. Rivkin, 394, (Academic, 2013).
- [3] K. Zacny et al. "Asteroids: anchoring and sample acquisition approaches in support of science, exploration, and in situ resource utilization," *Asteroids*. 758-801 (Springer 2013).
- [4] Ellis, Ralph (12 November 2014). "Philae touches down on the surface of a comet". CNN. Retrieved 12 November 2014.
- [5] Aron, Jacob (13 November 2014). "Problems hit Philae after historic first comet landing". New Scientist. Retrieved 13 November 2014.
- [6] Daniel J., Scheeres, "Sandcastles in space," *Nature* . 512, (Academic, 2014) 139-140.
- [7] B. Snow, "Some useful numbers on the engineering properties of materials (geologic and otherwise), <https://web.stanford.edu/tyzhu/Documents/Some20Useful20Numbers.pdf>, 20 October 2014, June 4,2009.
- [8] S.N. Batiste, "Geotechnical properties of lunar Regolith and Effects On Lunar Science Missions," (2008).
- [9] David S. McKay, *The Lunar Regolith Resources* (Academic, 1998).
- [10] Brad R. Blair, "Asteroid Mining Methods," SSI Space Manufacturing Conference (2010).
- [11] G.H. Heiken, D.T. Vaniman and B.M French,"Physical Properties of the Lunar Surface" in "*Lunar Sourcebook: a user's guide to the moon*" 483 (Academic, 1991)
- [12] Viorel Badescu, *Asteroids: Prospective Energy and Material Resources*, 470-494 (Academic, 2013).
- [13] Alshibli, K. and Hasan, A. (2009). "Strength Properties of JSC-1A Lunar Regolith Simulant." *J. Geotech. Geoenviron. Eng.*, 135(5), 673–679.
- [14] D.C. Baird, "Measurement and Uncertainty," in *Experimentation, An Introduction to Measurement Theory and Experiment Design*, 3rd Edition. Kingston, Canada. Eng., (Academic, 1995).